

## BIOMEDICINE

# Implantable bioelectronic systems for early detection of kidney transplant rejection

Surabhi R. Madhvapathy<sup>1,2</sup>, Jiao-Jing Wang<sup>3</sup>, Heling Wang<sup>4,5,6</sup>, Manish Patel<sup>2,7</sup>, Anthony Chang<sup>8</sup>, Xin Zheng<sup>3</sup>, Yonggang Huang<sup>4,5</sup>, Zheng J. Zhang<sup>3,9,10\*</sup>, Lorenzo Gallon<sup>3,11\*</sup>, John A. Rogers<sup>1,2,12,13†</sup>

Early-stage organ transplant rejection can be difficult to detect. Percutaneous biopsies occur infrequently and are risky, and measuring biomarker levels in blood can lead to false-negative and -positive outcomes. We developed an implantable bioelectronic system capable of continuous, real-time, long-term monitoring of the local temperature and thermal conductivity of a kidney for detecting inflammatory processes associated with graft rejection, as demonstrated in rat models. The system detects ultradian rhythms, disruption of the circadian cycle, and/or a rise in kidney temperature. These provide warning signs of acute kidney transplant rejection that precede changes in blood serum creatinine/urea nitrogen by 2 to 3 weeks and approximately 3 days for cases of discontinued and absent administration of immunosuppressive therapy, respectively.

**A**pproximately 60% of the 40,000 solid organ transplants performed in the US in 2022 were kidneys (1). However, human leukocyte antigen genotype mismatch between the donor and recipient can result in transplant rejection (2). Graft failure can occur at any time: 1-year, 5-year, and 10-year graft survival rates are 92.7, 77.6, and 49.5%, respectively, with rejection as the main cause of failure (3). Subclinical rejections can occur in 10 to 15% of renal transplant recipients within the first few months to a year post transplant (4–7).

Therapeutic intervention upon detection of early-stage rejection could preserve graft function. The current “gold standard” for detecting transplant rejection is a biopsy of the kidney cortex tissue, which has potential for complications such as bleeding, pain, infection, and accidental damage to adjacent organs (8). Biopsies are thus infrequent, typically performed 1 to 2 times in the first 24 months after transplantation or upon detection of elevated levels of serum creatinine/blood urea nitrogen (BUN)

(4, 5, 9). Factors unrelated to rejection, such as diet, muscle mass, infection, and medications also alter these biomarkers, leading to false-negative or -positive predictions of rejection (10). Moreover, changes in serum creatinine lag from days to weeks behind changes in glomerular filtration rate (GFR) (10). Other minimally invasive techniques offer significant advantages in sensitivity but are limited by drawbacks similar to those in blood collection such as restricted monitoring frequencies and the requirement for off-site analysis (11–18). There remains a clinical need for techniques that can continuously monitor graft health from the moment of transplantation and detect the onset or early stages of rejection, when serum creatinine/BUN are still within the normal physiological range (subclinical rejection).

During acute rejection, inflammatory events mediated by T-cell-generated cytokines and/or by allo-antibodies binding to tissue antigens take place within the transplanted organ. We report fully implantable, wireless bioelectronic systems capable of precise measurements of local organ temperature ( $T_{\text{kidney}}$ ) and thermal conductivity ( $k_{\text{kidney}}$ ) as biophysical surrogates for inflammation/perfusion in rat renal transplant models. The sensor interfaces directly with the curved, soft surface of the organ for continuous *in vivo* monitoring in freely moving animals from the moment of transplantation.

## Monitoring rat kidney transplant rejection

Kidney transplant models based on rats are suited for research because they are well-characterized, highly repeatable, and cost effective. The surgical procedures used in the following studies involve removing both native kidneys and grafting the transplanted kidney through the vascular anastomoses between the donor vessels and the abdominal aorta/inferior vena cava on the right side of

the body (Fig. 1A). The bioelectronic system, which is implanted after reperfusion of the grafted kidney, lies completely within the abdominal cavity and consists of a microfabricated, mechanically compliant biosensor that directly mounts on the surface of the kidney and connects by fine wires to a wireless electronics module secured to the adjacent abdominal wall. Additional images of the device and implantation appear in figs. S1 and S2.

The rat kidney is small ( $\sim 1 \times 1 \times 2 \text{ cm}^3$ ), soft [Young's modulus ( $Y$ )  $\sim 4.5 \text{ kPa}$ ] (19), and highly perfused [ $\sim 300 \pm 51.3 \text{ ml} \times \text{min}^{-1} \times (100 \text{ g tissue})^{-1}$ ] (20). The miniature ( $\sim 0.3 \times 0.7 \text{ cm}^2$ ), stretchable (20% stretchability, fig. S3A), flexible (bending radius  $\geq \sim 2.8 \text{ mm}$ , fig. S3B), ultrathin ( $\sim 220 \mu\text{m}$ ), and smooth ( $0.13 \mu\text{m} \pm 0.02$  areal surface roughness) design of the sensor allows for a gentle and seamless interface to the delicate surface of the kidney without risk of organ damage. The biosensor relies on lithographically patterned features of gold (100-nm thick,  $\sim 20\text{-}\mu\text{m}$  wide) to form a 3-mm diameter thermal sensing “disk” and a pair of serpentine interconnects (each  $\sim 80\text{-}\mu\text{m}$  wide), all encapsulated by layers of polyimide ( $10 \mu\text{m}$ ) and silicone ( $100 \mu\text{m}$ ) (figs. S4 and S5). The sensor contacts the dorsal kidney cortex beneath a tight “pocket” formed under the  $\sim 25 \mu\text{m}$  thick renal capsule (21) and is sutured to it [Fig. 1, A (inset) and B]. The electronics module contains sensor readout circuitry and a bluetooth low energy system-on-chip for control and data transmission, with a coin-cell battery for power supply (fig. S6). The small lateral dimensions ( $\sim 1.1 \times 1.6 \text{ cm}^2$ ), thickness ( $\sim 0.5 \text{ cm}$ ), and smooth surface of the electronics module facilitate insertion within the abdominal cavity (Fig. 1C). Details on the measurement appear in the methods section and figs. S7 to S9. Real-time, continuous data collection in untethered, freely moving animals, with stable operation is possible for 2 months or more (fig. S10) without adverse effects.

Measurements of  $T_{\text{kidney}}$  and  $k_{\text{kidney}}$  performed using this system for  $t = 27$  days in the native (right) solitary kidney of a control animal highlight effects of surgical recovery and natural biological variations (Fig. 1D).  $T_{\text{kidney}}$  increases rapidly after the anesthesia wears off ( $t = 0 \text{ days}$ ) to a peak value  $\sim 3$  to 4 hours post surgery ( $\sim 39^\circ\text{C}$ ) and then subsequently decreases, concurrent with the release of post-operative analgesia to an average value of  $\sim 37.5^\circ\text{C}$ . The irregular pattern in  $T_{\text{kidney}}$  between  $t = 0$  to 2 days arises from post-operative recovery and from the influence of a heating pad under one side of the animal cage to assist with body temperature regulation. Details of the effects of this pad and of the ambient temperature are in fig. S11; variations in the ambient temperature do not influence  $T_{\text{kidney}}$ . A periodic  $\sim 1\text{-day}$  circadian rhythm emerges

<sup>1</sup>Department of Materials Science and Engineering, Northwestern University, Evanston, IL, USA 60208. <sup>2</sup>Querry Simpson Institute for Bioelectronics, Northwestern University, Evanston, IL, USA 60208. <sup>3</sup>Comprehensive Transplant Center, Northwestern University, Chicago, IL, USA 60611. <sup>4</sup>Department of Mechanical Engineering, Northwestern University, Evanston, IL, USA 60208. <sup>5</sup>Department of Civil Engineering, Northwestern University, Evanston, IL, USA 60208. <sup>6</sup>Laboratory of Flexible Electronics Technology, Tsinghua University, Beijing, 100085 China. <sup>7</sup>Department of Intervention Radiology, University of Illinois at Chicago, Chicago, IL, USA 60612. <sup>8</sup>Department of Pathology, University of Chicago, Chicago, IL, USA 60637.

<sup>9</sup>Department of Surgery, Northwestern University Feinberg School of Medicine, Chicago, IL, USA 60611. <sup>10</sup>Simpson Querry Institute for BioNanotechnology, Northwestern University, Chicago, IL, USA 60611. <sup>11</sup>Department of Nephrology, Northwestern University, Chicago, IL, USA 60611. <sup>12</sup>Department of Biomedical Engineering, Northwestern University, Evanston, IL, USA 60208. <sup>13</sup>Department of Neurological Surgery, Northwestern University, Chicago, IL, USA 60611.

\*Corresponding author. Email: zjzhang@northwestern.edu (Z.J.Z.); lgallon@northwestern.edu (L.G.); jrogers@northwestern.edu (J.A.R.)  
†These authors contributed equally to this work.

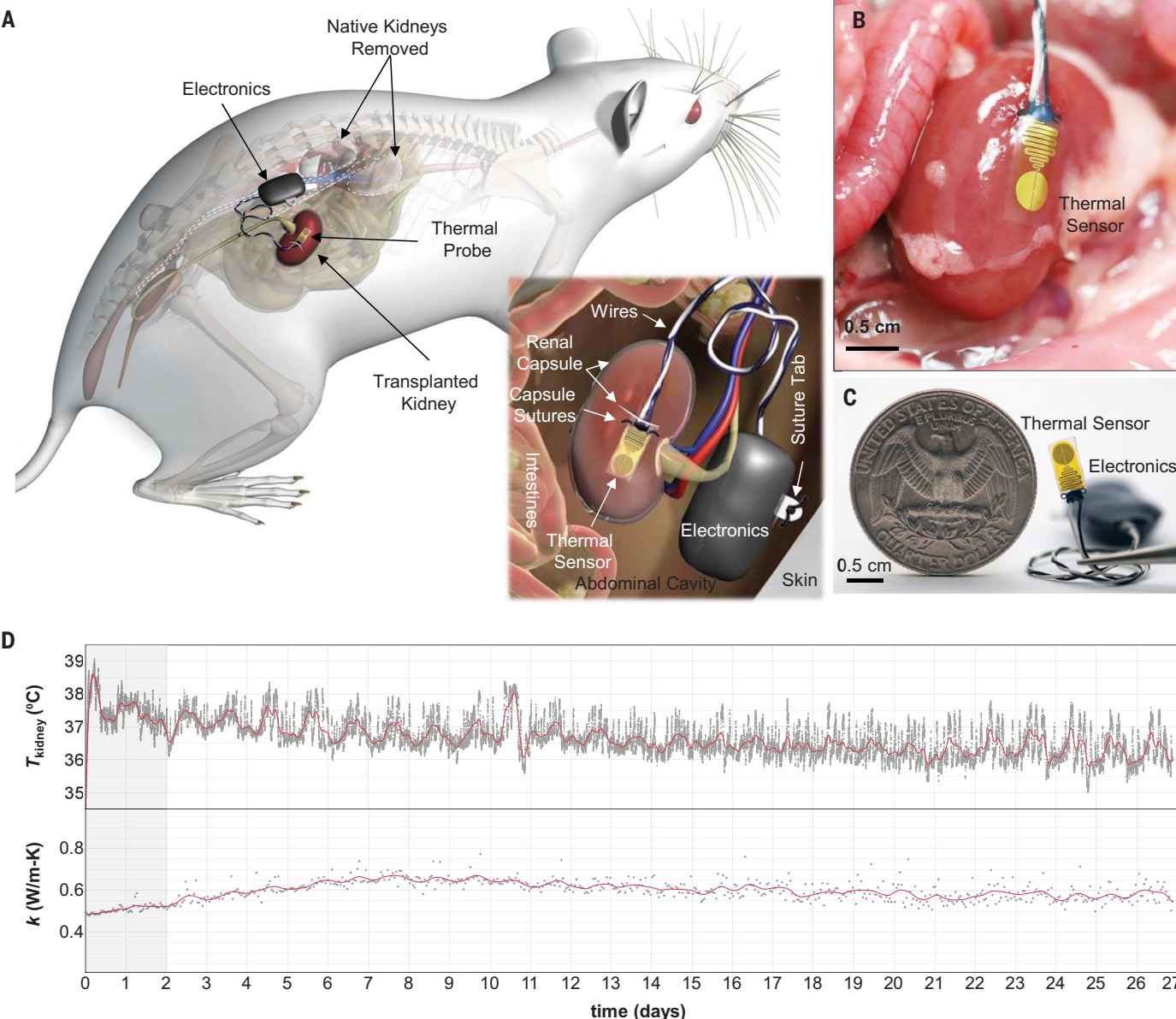


**Fig. 1. Monitoring kidney transplant rejection using an implantable bioelectronic system.** (A) Illustration of kidney transplant and device implantation in a rat model. The dashed white lines highlight removal of both native kidneys. The sensor directly interfaces with the cortex, sutured to the overlying renal capsule through two suture holes (inset). The electronics reside adjacent to the kidney, secured to the abdominal wall through a suture tab. The wires connecting the sensor and electronics

module lie against the abdominal fat. Photograph of (B) the sensor implanted on the dorsal side of the kidney and (C) the device next to a US Quarter (scale bar = 5 mm). (D) Time variation of the organ temperature ( $T_{\text{kidney}}$ ) and thermal conductivity ( $k_{\text{kidney}}$ ) collected for a Lewis rat with a single native kidney (second kidney nephrectomized) and for  $t = 0$  to 28 days. The gray points represent the raw data. The red line is a smoothing spline fit ( $\lambda = 0.01$ ).

after  $t = 2$  days, consistent with the return to a healthy behavioral pattern. The bioelectronic system has no measurable effect on grooming, activity, food and water consumption, or sleep/wake cycles. Short-term (~40 min to 1 hour) variations in  $T_{\text{kidney}}$  are correlated with motion/activity (fig. S12).

$k_{\text{kidney}}$  is a function of perfusion and the tissue thermal properties, increasing from ~0.48 W/m-K to a final value of ~0.64 W/m-K over  $t = 0$  to 6 days.  $k_{\text{kidney}}$  at  $t = 6$  days for an animal with both native kidneys intact (fig. S13) is

approximately half (~0.33 W/m-K) that of an animal with a single native kidney, consistent with the understanding that the vascular load of the body splits equally between the two kidneys. These observations in control animals provide a point of reference for the studies on transplant rejection.

#### Characterization of acute kidney transplant rejection

Renal transplantation between inbred rat strains with different major histocompat-

ability complexes (MHC) provides control over transplant acceptance or rejection. Lewis Rats (MHC haplotype RT1<sup>l</sup>) are both the donors and recipients in isogenic transplants (Fig. 2A). Isogenic transplants are analogous to those between identical twins in humans and result in graft acceptance without the need for immunosuppression. August-Copenhagen-Irish (ACI) rats (MHC haplotype RT1<sup>av1</sup>) are the donors and Lewis rats are the recipients in allogeneic transplants (Fig. 2B). Allotransplants, which represent the

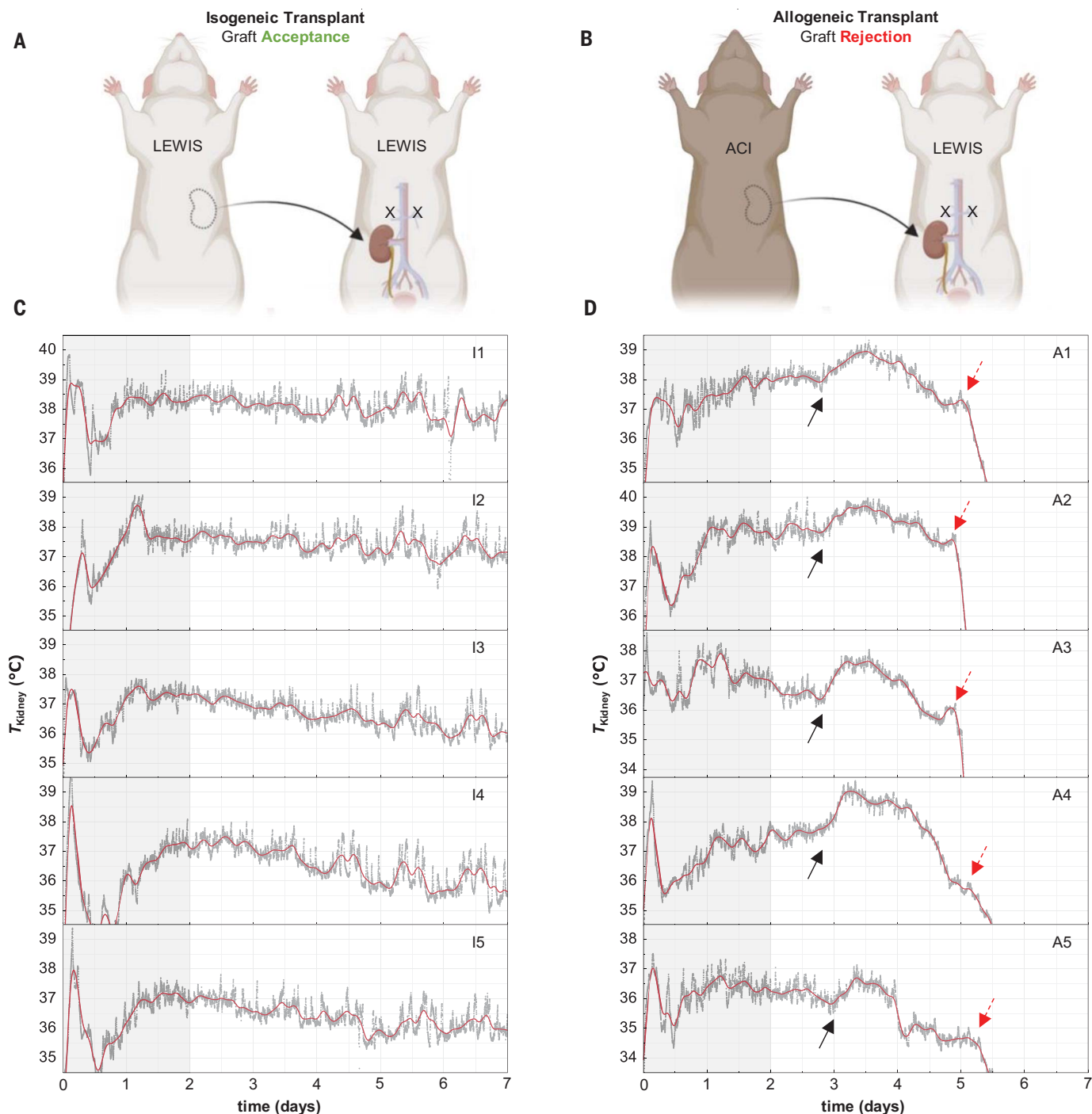


**Fig. 2. Characterization of acute rejection.** Illustrations of a rat kidney transplantation model using inbred rat strains for (A) isogeneic transplant, where both the donor and recipient strains are Lewis rats, leading to graft acceptance and (B) allogeneic transplant, where the donor strain is the August Copenhagen Irish (ACI) rat and the recipient is a Lewis rat, resulting in graft rejection. “X” denotes the removal of both recipient native kidneys.  $T_{\text{kidney}}$  measured for ~7 days for (C)  $n = 5$  isografts and (D)  $n = 5$  allografts. In this and subsequent figures, labels (e.g., A1-5, I1-5)

most clinically relevant cases for humans, result in graft rejection. The survival time for ACI-to-Lewis transplants is ~8 days without immunosuppressive medication (22). Details of the procedures are in the methods section.

$T_{\text{kidney}}$  for isografts varies until  $t \sim 3$  days as a result of induced inflammation, effects of analgesia, and post-operative care (Fig. 2C). A circadian rhythm emerges after  $t \sim 3$  days. The average daily  $T_{\text{kidney}}$  remains constant after

identify each individual dataset (table S1). The gray points represent the raw data. The red line is a smoothing spline fit ( $\lambda = 0.01$ ). The shaded region ( $t = 0$  to 2 days) indicates the post-surgery recovery period during which a heating pad placed underneath half of the animal cage assists with thermoregulation. The black arrows in Fig. 2D correspond to a feature in  $T_{\text{kidney}}$  (bump and inflection point) unique to the allografts at  $t \sim 3$  days. The red arrows in Fig. 2D correspond to a sharp decrease in  $T_{\text{kidney}}$  at  $t \sim 5$  days.

$t \sim 7$  days (data >7 days is in fig. S14). Trends in  $T_{\text{kidney}}$  and overall behaviors are consistent for all  $n = 5$  animals, similar to those of control animals with native kidney(s) (Fig. 1E and fig. S13). Minimal adhesions/foreign body response

(FBR) appear on the surface of the kidney or around the sensor, interconnecting wires, or electronics module at the experimental end point (21 to 28 days) (fig. S15). The response time ( $t_{90}$ ) of the biosensor for measurements of temperature is 0.13 s (fig. S16). Growth of FBR on chronic timescales (23) increases this response time ( $t_{90} = 1.49$  s for a fibrotic capsule thickness of 250  $\mu\text{m}$ ) but does not affect measurement sensitivity to  $T_{\text{kidney}}$  (fig. S17). These observations suggest that the graft is healthy, without adverse effects induced by the bioelectronic system.

$T_{\text{kidney}}$  for allografts bears little resemblance to the data for isografts (Fig. 2D). For all allografts ( $n = 5$ ),  $T_{\text{kidney}}$  rises at  $t \sim 3$  days for a period of  $\sim 18$  hours and then decreases over the subsequent  $\sim 18$  hours.  $T_{\text{kidney}}$  decreases sharply (approximately  $-0.5^\circ\text{C}$  per hour) around  $t \sim 5$  to 6 days and 30 to 32°C, which establishes the experimental end point (full temperature range appears in fig. S18). Lack of food/water intake and locomotion characterize behaviors during the  $T_{\text{kidney}}$  decline on day 5/6 (fig. S12). At the end point, adhesions and FBR surround the graft, which is enlarged ( $\sim 1.5$  to 2 times the original size) and has a marbled appearance with necrotic patches distinctive of acute rejection (fig. S15). The impact of patchy or focal rejection on  $T_{\text{kidney}}$  appears in fig. S19.

The results for  $k_{\text{kidney}}$  for all isografts and allografts (fig. S20) are similar to those for a single healthy kidney ( $\sim 0.64$  W/m·K), as observed in fig. S13. In addition,  $k_{\text{kidney}}$  decreases with time for 3/5 allotransplants, consistent with the severe FBR observed at the end point for these cases. Unlike  $T_{\text{kidney}}$ ,  $k_{\text{kidney}}$  does not display systematic trends that distinguish allografts from isografts. A drop in GFR may be obscured by any comparatively small change in perfusion/associated kidney tissue damage due to the rejection response. Second, the speckled/irregular color of rejected kidneys suggests that changes in perfusion, tissue necrosis, or other effects that can alter  $k_{\text{kidney}}$  may be localized and nonuniform over the kidney surface. In such cases, the measurements would depend on the relative size and exact position of the biosensor, in ways that are difficult to control systematically.

#### Organ temperature provides an early warning sign of transplant rejection

Correlating  $T_{\text{kidney}}$  with histological and blood biomarker analysis is essential for evaluating its significance and utility for detecting graft rejection. The following discussion (Fig. 3) focuses on two separate time points coinciding with the allograft  $T_{\text{kidney}}$  features identified in Fig. 2D: (i)  $t = 5$  to 6 days (referred to as the end point) corresponding to the steep temperature decline and (ii)  $t = 3$  to 4 days (referred to as the midpoint) corresponding to the inflection point and tran-

sitory rise and fall (i.e., “bump”). Isograft data serve as the control reference. Macroscopic and microscopic histological examination at the end point reveals that the kidney is normal for isografts and acutely rejected for allografts (Fig. 3, A and B, and extended data in figs. S21 and S22). Diffuse cortical necrosis and thrombotic microangiopathy—characteristic of severe acute rejection—appear in 4 of the 5 allografts. The fifth allograft exhibits type I tubulointerstitial rejection. BUN and creatinine levels are within the normal range for Lewis rats in the case of isografts (Fig. 3, C and D) but are highly elevated for allografts ( $P < 0.0001$  and  $P < 0.0003$ , respectively). The high value of BUN ( $>140$  mg/dl) for allografts indicates uremia, consistent with behavioral characteristics including signs of pain, slowed or absent motion, and reduced food and water intake.  $\bar{T}_n$  denotes the average  $T_{\text{kidney}}$  between day  $n$  and  $n - 1$ . The temperature decline for the allografts, denoted by the difference in average  $T_{\text{kidney}}$  on the final and penultimate days of survival ( $\bar{T}_6 - \bar{T}_5$ ), is also significant ( $P = 0.0122$ ) (Fig. 3E). Thus, behavioral, blood marker, and  $T_{\text{kidney}}$  analysis accurately detect late-stage graft rejection at the end point, as verified by histology.

Evaluations of the data at the midpoint offer physiological insight into the origin of the  $T_{\text{kidney}}$  inflection point and bump seen in Fig. 2D. A separate set of experiments involves harvesting allograft and isograft kidneys close to the midpoint for this purpose ( $T_{\text{kidney}}$  and  $k_{\text{kidney}}$  data in fig. S23). For  $n = 3$  cases each, histological examination reveals that the isografts have normal morphology whereas all allografts exhibit type I tubulointerstitial rejection (representative cases in Fig. 3, F and G; remaining data shown in fig. S24). The allograft case presented in Fig. 3G, harvested exactly at the inflection point ( $t \sim 3$  days), displays mild type I tubulointerstitial rejection, demonstrating that the allograft  $T_{\text{kidney}}$  bump coincides with the histological onset of rejection.

By comparison, BUN and serum creatinine levels at the midpoint ( $t = 4$  days) do not offer clear diagnostic value, as the difference in values for isografts ( $n = 4$ ) and allografts ( $n = 6$ ) is not statistically significant (Fig. 3, H and I). By contrast,  $(\bar{T}_4 - \bar{T}_3)$ , which is an indicator of the height of the bump, is larger for allografts ( $\sim 0.6^\circ\text{C}$ ) compared to isografts (approximately  $-0.3^\circ\text{C}$ ) ( $P = 0.0016$ ,  $n = 5$ ) (Fig. 3J). The bump therefore identifies acute rejection at an earlier time point than does BUN or serum creatinine. The absolute height and width of the allograft bump ( $n = 5$ ) are  $\sim 1.0 \pm 0.2^\circ\text{C}$  and  $\sim 1.8 \pm 0.4$  days, respectively. The onset of the bump occurs at  $2.8 \pm 0.1$  days. Animal behavior for allografts at  $t \sim 4$  days appears normal and is indistinguishable from isografts. Thus, continuous measurements of

$T_{\text{kidney}}$  show potential for detection of acute rejection before signs of loss of graft function appear in blood markers or behavioral patterns. These features in  $T_{\text{kidney}}$  are unlike those observed in body  $T$  of rodent models of induced septic shock (24–27) or in  $T_{\text{kidney}}$  during renal ischemia reperfusion injury (fig. S25 and table S2).

#### Delayed graft rejection with immunosuppressants

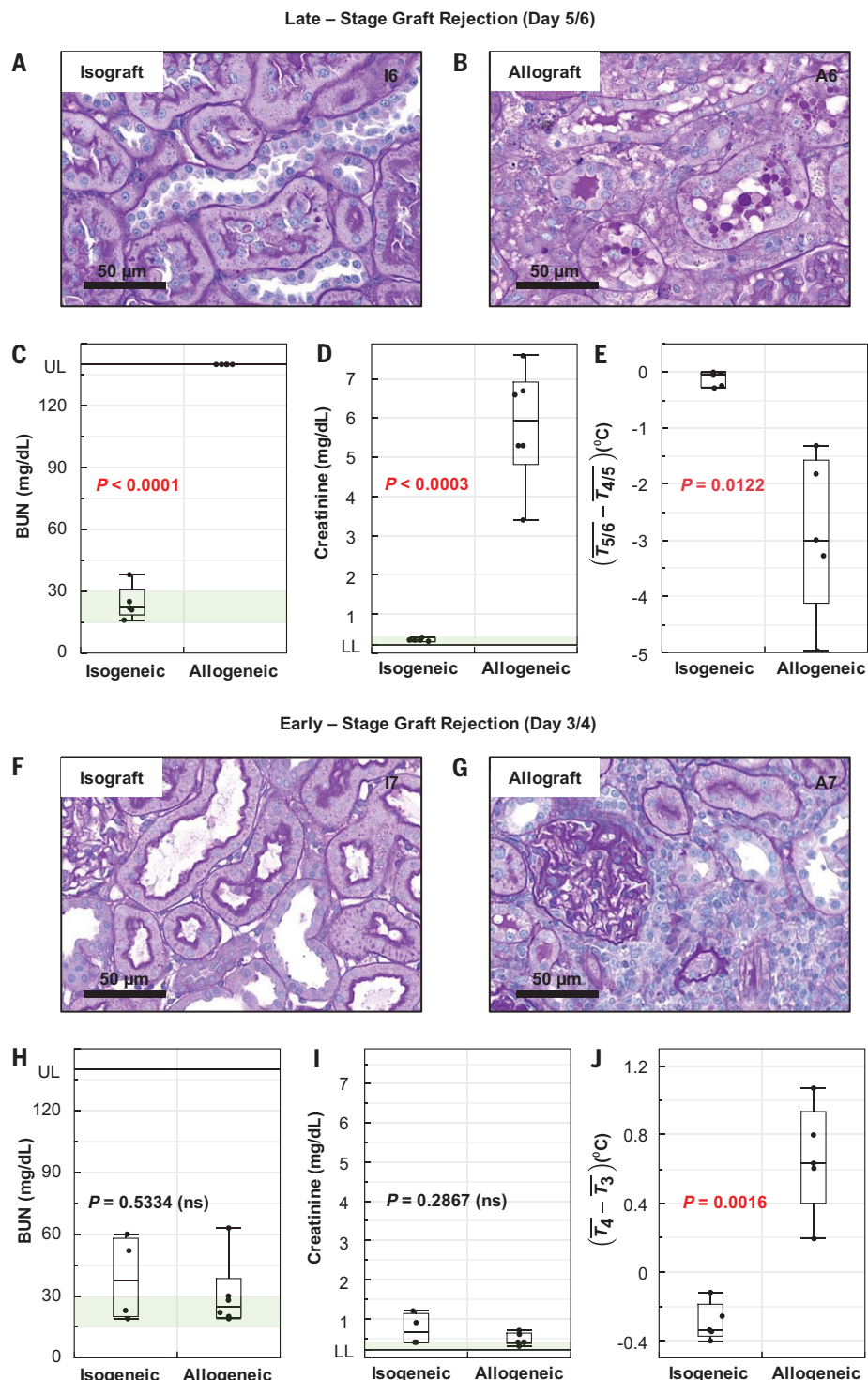
Real-world kidney allotransplants require immunosuppressants to inhibit graft rejection. The following experiments (Fig. 4) mimic clinical cases of patient noncompliance, where patients prematurely stop or reduce their prescribed immunosuppressant dose. Allografts receive 1 mg/kg per day FK506 for  $t = 0$  to 7 days through a subcutaneously implanted osmotic pump (2ML1, Alzet, Inc.) (Fig. 4A). The recordings include both  $T_{\text{kidney}}$  and  $k_{\text{kidney}}$  for one case, and measurements of only  $T_{\text{kidney}}$  for the other cases, using a simplified version of the device placed in contact with the kidney (fig. S26 showcases correlation for the gold versus contact sensor). This simplified device has extended battery lifetime (details in Methods). The time evolution of renal function (collected at fixed times  $t \sim 4, 7, 10, 14, 21$ , and 27 days) illustrates that creatinine and BUN rise above normal levels only at  $t \geq 27$  days (Fig. 4B), coincident with a  $\sim 9\%$  decline in body weight (fig. S27).

$T_{\text{kidney}}$  from isografts serves as a point of reference for medicated allograft data (Fig. 4C). Data from allografts treated with 1 mg/kg FK506 exhibit several notable features that are unlike those observed in isografts (Fig. 4, D to H). After the initial  $t = 0$  to 2 day surgical recovery phase,  $T_{\text{kidney}}$  remains flat until  $t \sim 7$  days, with minimal variations and no circadian cycle, concurrent with the administration period of FK506. An inflection point at  $t \sim 8$  to 9 days appears in 4 of the 5 animals (Fig. 4, D to G).  $T_{\text{kidney}}$  slowly rises and reaches a peak at  $t = 14$  days, followed by a slow decline (a “bump”). At  $t \sim 22$  days,  $T_{\text{kidney}}$  falls steeply (approximately  $-0.83^\circ\text{C}$  per day on average). Data from medicated allograft cases also present additional higher frequency components relative to isografts. Data collected beyond  $t = 28$  days, up to 2.5 months, appears in fig. S28.

Histopathology offers insight into kidney health at the time points corresponding to the occurrence of key features in  $T_{\text{kidney}}$  in Fig. 4, D to H (“bump”, high-frequency components). Extended histology data and  $T_{\text{kidney}}$  for experiments that involve harvesting the kidney at earlier time points are in figs. S29 and S30. The kidney at  $t \sim 10$  days is not rejected (Fig. 4I). At the peak in temperature ( $t \sim 14$  days), and at  $t = 21$  and 27 days, type I acute tubulointerstitial rejection occurs, characterized by

**Fig. 3. Kidney temperature as an early indicator of acute rejection.**

**Representative periodic acid-schiff (PAS)-stained histological section for an (A) isograft at  $t = 6$  days, displaying normal parenchyma with back-to-back arrangement of tubules, normal glomeruli, and an absence of interstitial inflammation and (B) allograft at  $t = 6$  days, with severe type I rejection characterized by prominent interstitial inflammation with tubulitis. Allografts show elevated (C) BUN and (D) serum creatinine levels at  $t \sim 6$  days relative to isografts. UL and LL denote the upper and lower detection limits of the analyzer.  $\bar{T}_n$  represents  $T_{\text{kidney}}$  averaged over  $t = n - 1$  to  $t = n$  days. (E) Allografts show lower ( $\bar{T}_{5/6} - \bar{T}_{4/5}$ ) than isografts ( $n = 5$ ). PAS-stained histological sections show that at  $t \sim 4$  days, (F) the isograft kidney is normal whereas (G) the allograft kidney shows signs of type I acute rejection. (H) BUN and (I) serum creatinine at  $t \sim 4$  days are not significantly different (ns) between allografts and isografts (J) ( $\bar{T}_4 - \bar{T}_3$ ) is a statistically significant metric for the  $T_{\text{kidney}}$  bump in Fig. 2D ( $n = 5$ ). The green shaded region in Fig. 3, E, F, H, and I represent normal levels for Lewis rats without transplant.**



diffuse interstitial inflammation and tubulitis. All five medicated allografts (FK 1 mg/kg) display histological evidence of rejection at the end points (Fig. 4, D to H).

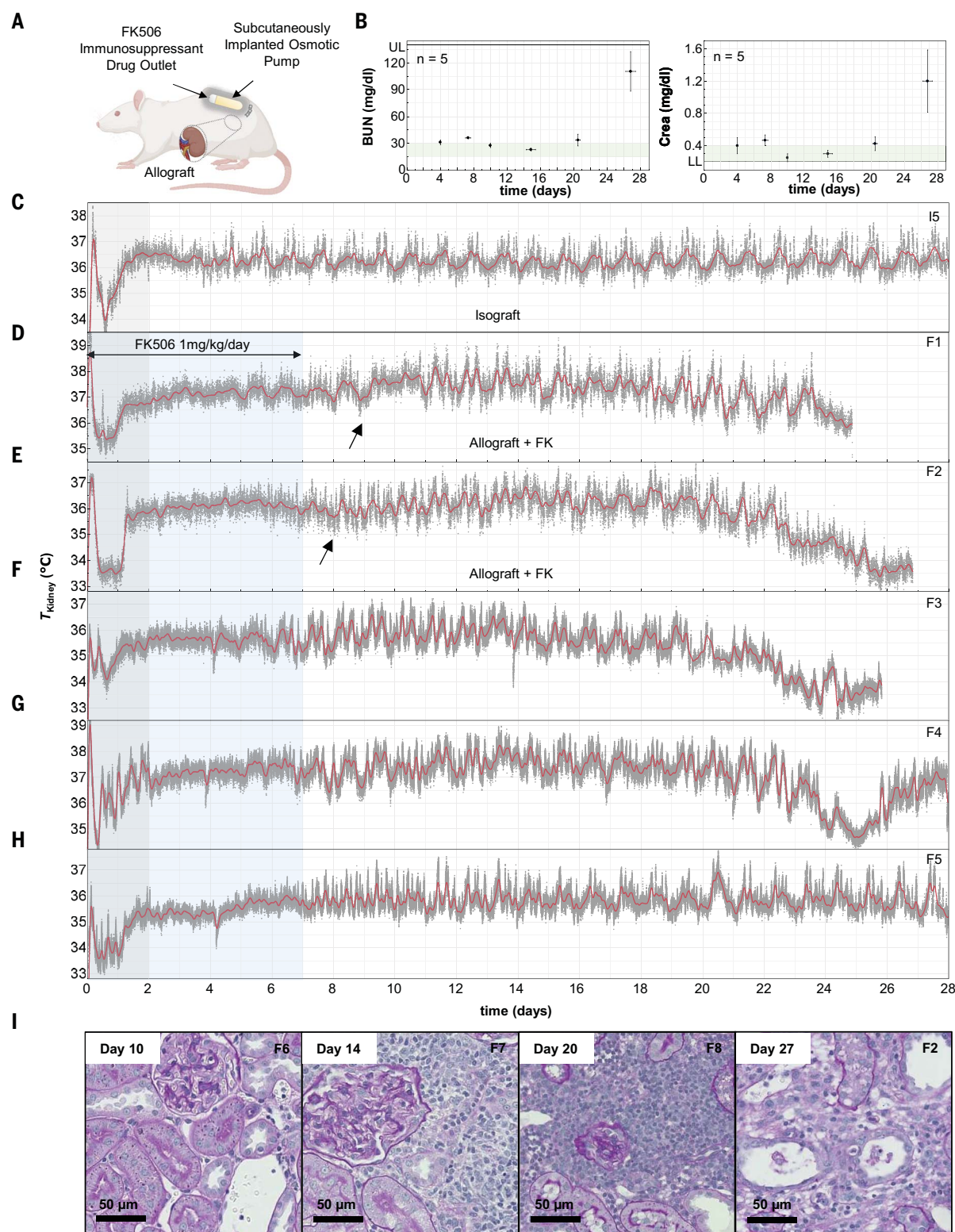
**Early indication of acute rejection**

The bump observed for data from medicated allografts can be characterized by a statisti-

cally significant temperature rise ( $\bar{T}_{14} - \bar{T}_{10}$ ) and decline ( $\bar{T}_{20} - \bar{T}_{14}$ ) (median rise  $\sim 0.15^{\circ}\text{C}$ ,  $P = 0.0353$ , median decline approximately  $-0.3^{\circ}\text{C}$ ,  $P = 0.0184$ ) compared to isografts (Fig. 5A,B), and are “muted” relative to the unmedicated allografts ( $\sim -0.6^{\circ}\text{C}$ ). Blood markers fail to detect rejection until  $t \geq 27$  days. This time point is much later than the onset of rejection,

which occurs between  $t = 10$  and 14 days as evidenced by histology (Fig. 4B and 4I).

Fourier transform analysis of  $T_{\text{kidney}}$  for  $t = 7$  to 21 days (corresponding to the post-medication period, inflection point, and coinciding with the muted bump) reveals the presence of strong ultradian ( $f > 1 \text{ day}^{-1}$ ) rhythms (specifically,  $f = 2 \text{ day}^{-1}$ ) for all medicated allografts relative

**Fig. 4. Delayed rejection after discontinuation of immunosuppressants.**

(A) Illustration of the delivery of FK506 to an allograft at a continuous dose of 1 mg/kg per day for  $t = 0$  to 7 days. (B) Serum creatinine and BUN collected at discrete time points ( $t \sim 4, 7, 10, 14, 20$ , and 27 days) for animals treated with FK506. (C)  $T_{\text{kidney}}$  versus  $t$  for a representative isograft for 28 days. (D to H)  $T_{\text{kidney}}$  versus  $t$  for  $n = 5$  allografts treated with 1 mg/kg per day FK506 for  $t = 0$  to 7 days (treatment period denoted by blue shaded region). The gray shaded region ( $t = 0$

to 2 days) indicates the post-surgery recovery period. The gray points represent the raw data. The red curve is a smoothing spline fit ( $\lambda = 0.01$ ). The black arrows correspond to the onset of a muted temperature bump. (I) Representative histological sections stained with PAS for a harvested kidney at  $t = 10$  days shows normal kidney parenchyma without any features of acute rejection whereas those at  $t = 14, 20$ , and 27 days all demonstrate acute type I tubulointerstitial rejection, characterized by diffuse interstitial inflammation and frequent tubulitis.

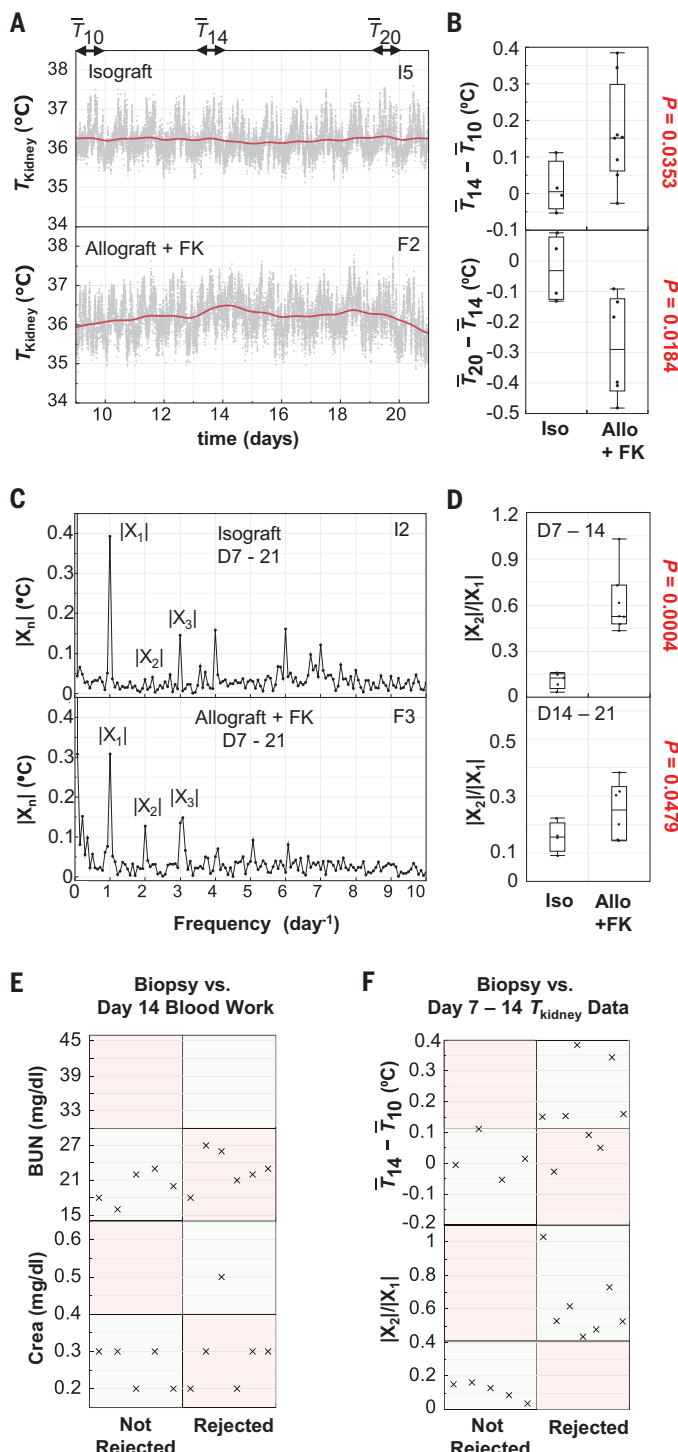


**Fig. 5. Temperature as an early indicator of rejection relative to blood markers.** (A)  $T_{\text{kidney}}$  for a representative isograft and allograft for  $t = 9$  to 21 days. Gray points represent the raw data. The red curve is a smoothing spline fit ( $\lambda = 30$ ). (B) The bump rise ( $\bar{T}_{14}$  to  $\bar{T}_{10}$ ) and subsequent decline ( $\bar{T}_{20}$  to  $\bar{T}_{14}$ ) are significant in medicated allografts compared to isografts ( $n = 5$ ). (C) Fourier Transform of the  $T_{\text{kidney}}$  data from fig. S14 and Fig. 4F. (D) The ratio of the magnitudes of the  $f = 2 \text{ day}^{-1} |X_2|$  and  $f = 1 \text{ day}^{-1} (|X_1|)$  peaks for  $t = 7$  to 14 days (top) and  $t = 14$  to 21 days (bottom) is greater in medicated allografts relative to isografts ( $n = 5$ ). (E) Confusion matrices comparing the measured values of BUN and creatinine in isografts and medicated allografts to histological diagnosis. (F) Confusion matrix comparing  $(\bar{T}_{14} - \bar{T}_{10})$  and  $|\frac{|X_2|}{|X_1|}|$  to blinded histological diagnosis. The cutoff values in (E) are the upper limits of normal BUN and Creatine for Lewis rats and in (F) are the corresponding grand means of the datasets. The red shaded regions correspond to false-positive and -negative evaluations, and the green shaded regions are true negative and positive outcomes.

to isografts (Fig. 5C). The ratio of amplitudes of the half-day and circadian cycles ( $|\frac{|X_2|}{|X_1|}|$ ) is statistically significant between  $t = 7$  to 14 days ( $P = 0.0004$ ) and remains so between  $t = 14$  to 21 days ( $P = 0.0479$ ) (Fig. 5D). Similarly, ( $|\frac{|X_3|}{|X_1|}|$ ) is also statistically significant (fig. S31). The presence of stronger ultradian features in medicated allografts may be a result of the cyclic nature of T cell activity and/or cellular repair/damage processes, synced with the circadian clock (28–30).

The subclinical relevance of  $T_{\text{kidney}}$  and creatinine/BUN can be established by comparison with histology. Accuracy and true positive rate (TPR) calculated from confusion matrices of BUN (accuracy = 46%, TPR = 0%) and creatinine levels (accuracy = 54%, TPR = 17%) illustrate that blood markers cannot detect early-stage or onset of rejection ( $t = 14$  days); nearly all medicated allografts result in false negatives (Fig. 5E). On the other hand, features in  $T_{\text{kidney}}$  such as the bump (accuracy = 75%, TPR = 62%) and the half-day ultradian rhythm (accuracy = 100%, TPR = 100%) correctly identify early-stage or onset of rejection (Fig. 5F).

## Conclusions

This study in rat transplantation models establishes biophysical measurements of  $T_{\text{kidney}}$  and  $k_{\text{kidney}}$  as a technique to detect subclinical acute rejection. Compared to invasive biopsies, these biosensors offer dense, real-time, long-term information about surgical recovery, impact of medications, circadian/ultradian rhythms, motion/activity, and graft rejection.  $T_{\text{kidney}}$  provides early warning of rejection and greater sensitivity relative to serum creatinine and BUN, ~2 to 3 weeks and ~3 days in advance in cases of discontinued and absent administration of immunosuppressive therapy, respectively. Such measurements may help guide personalized dosing strategies and in understanding the efficacy of immunosuppressants.

## REFERENCES AND NOTES

1. K. L. Lentine et al., *Am. J. Transplant.* **22** (suppl. 2), 21–136 (2022).
2. L. D. Cornell, R. N. Smith, R. B. Colvin, *Annu. Rev. Pathol.* **3**, 189–220 (2008).
3. U.S. Department of Health and Human Services, National Institutes of Health, National Institutes of Health, National Institute of Diabetes and Digestive and Kidney Diseases, “2021 Annual Data Report” (USRDS, 2021); <https://usrds.adm.nih.gov/2021>.
4. T. Y. Kee et al., *Transplantation* **82**, 36–42 (2006).
5. D. N. Rush, S. F. Henry, J. R. Jeffery, T. J. Schroeder, J. Gough, *Transplantation* **57**, 208–210 (1994).
6. W. Zhang et al., *J. Am. Soc. Nephrol.* **30**, 1481–1494 (2019).
7. R. Mehta et al., *Am. J. Transplant.* **18**, 1710–1717 (2018).
8. K. Bakdash et al., *Semin. Intervent. Radiol.* **36**, 97–103 (2019).
9. D. J. Lo, B. Kaplan, A. D. Kirk, *Nat. Rev. Nephrol.* **10**, 215–225 (2014).
10. C. L. Edelstein, in *Biomarkers of Kidney Disease (Second Edition)*, C. L. Edelstein, Ed. (Academic Press, 2017), pp. 241–315.
11. Q. D. Mac et al., *Nat. Biomed. Eng.* **3**, 281–291 (2019).
12. P. J. O’Connell, K. L. Keung, M. C. Menon, B. Murphy, in *Kidney Transplantation - Principles and Practice (Eighth Edition)*, S. J. Knechtle, L. P. Marson, P. J. Morris, Eds. (Elsevier, 2019), pp. 418–433.
13. R. D. Bloom et al., *J. Am. Soc. Nephrol.* **28**, 2221–2232 (2017).

14. J. J. Friedewald *et al.*, *Am. J. Transplant.* **19**, 98–109 (2019).
15. R. El Fekih *et al.*, *J. Am. Soc. Nephrol.* **32**, 994–1004 (2021).
16. M. Naesens, D. Anglicheau, *J. Am. Soc. Nephrol.* **29**, 24–34 (2018).
17. E. Van Loon *et al.*, *Am. J. Transplant.* **21**, 740–750 (2021).
18. M. Suthanthiran *et al.*, *N. Engl. J. Med.* **369**, 20–31 (2013).
19. J.-L. Gennissen *et al.*, “Multiwave technology introducing shear wave elastography of the kidney: Preclinical study on a kidney fibrosis model and clinical feasibility study on 49 human renal transplants” in *2010 IEEE International Ultrasonics Symposium*, pp. 1356–1359 (2010).
20. C. A. Romero *et al.*, *Am. J. Physiol. Renal Physiol.* **314**, F99–F106 (2018).
21. R. N. Raman *et al.*, *J. Biomed. Opt.* **14**, 020505 (2009).
22. J. Schneiderman *et al.*, *Sci. Rep.* **12**, 7298 (2022).
23. J. C. Doloff *et al.*, *Nat. Biomed. Eng.* **5**, 1115–1130 (2021).
24. O. Laitano *et al.*, *Shock* **50**, 226–232 (2018).
25. S. Ebong *et al.*, *Infect. Immun.* **67**, 6603–6610 (1999).
26. K. D. Vlach, J. W. Boles, B. G. Stiles, *Comp. Med.* **50**, 160–166 (2000).
27. L. L. Monroe *et al.*, *Shock* **46**, 723–730 (2016).
28. M. Perelis, M. L. Ford, X. Luo, *Am. J. Transplant.* **15**, 293 (2015).
29. X. Yu *et al.*, *Science* **342**, 727–730 (2013).
30. G. Fernandes, in *Biologic Rhythms in Clinical and Laboratory Medicine*, Y. Touitou, E. Haus, Eds. (Springer, 1992), pp. 493–503.

#### ACKNOWLEDGMENTS

This work made use of the NUFAB facility of Northwestern University's NUANCE Center, which has received support from the SHyNE Resource (NSF ECCS-2025633), the IIN, and

Northwestern's MRSEC program (NSF DMR-1720139). This work made use of the Microsurgery and Preclinical Research Core Facility in the Comprehensive Transplant Center at the Feinberg School of Medicine. The authors thank J. Zhu, S. Coughlin, and J. Winograd for preliminary efforts in microfabrication. The authors thank A. Spann (Center for Advanced Molecular Imaging, Northwestern University) for 3D reconstruction of and segmentation of the contrast-CT image. The authors thank D. Procissi and N. Bertolino (Small Animal Imaging Facility, Center for Translational Imaging, Northwestern University) for collection of CT images. We thank M. Arceta, J. Hernandez, and S. Popovics for assistance with animal husbandry and care (Center for Comprehensive Medicine, Northwestern University). The authors acknowledge the Northwestern Mouse Histology and Phenotyping Laboratory for preparation of histological samples and the Northwestern Pathology Core Facility for assistance with scanning of histology slides. Figures 2A, 2B, and 4A were created by using Biorender.com. Illustrations in Fig. 1A were created by J. Sinn-Hanlon, iLearning@VetMed, UIUC. The authors thank J. Ciatti for the photograph in Fig. 1C and for performing surface roughness measurements. **Funding:** S.R.M. acknowledges support from the NSF Graduate Research Fellowship (NSF DGE-1842165). M.P. acknowledges support in part by an Alpha Omega Alpha Carolyn L. Kuckein Student Research Fellowship. **Author contributions:** Project conceptualization: S.R.M., J.A.R., and L.G. Design of hardware/software: S.R.M. Thermal sensor fabrication/calibration: S.R.M. Theoretical simulations: H.W. with guidance from Y.H. Design of Experiments: S.R.M., J.A.R., Z.J.Z., and L.G. Data analysis: S.R.M. with

review by J.A.R., Z.J.Z., and L.G. Surgeries: J.-J.W. and X.Z. with assistance from S.R.M. Animal blood draws/small procedures: J.-J.W. with assistance from S.R.M. and M.P. Post-operative care, monitoring of animals: S.R.M., M.P., and J.-J.W. Blinded Histology Review and Diagnosis: A. C. Project Supervision: J.A.R. and L.G. Original manuscript draft and figure preparation: S.R.M. Draft editing: S.R.M., J.A.R., L.G., and Z.J.Z. All authors read and provided comments on the manuscript. **Competing interests:** J.A.R., S.R.M., L.G., and Z.J.Z. have filed for a patent based on the research in this manuscript (PCT/US2023/010402).

**Data availability:** All data are available in the manuscript or the supplementary materials. **License information:** Copyright © 2023 the authors, some rights reserved; exclusive licensee American Association for the Advancement of Science. No claim to original US government works. <https://www.sciencemag.org/about/science-licenses-journal-article-reuse>

#### SUPPLEMENTARY MATERIALS

[science.org/doi/10.1126/science.adh7726](https://science.org/doi/10.1126/science.adh7726)  
Materials and Methods  
Figs. S1 to S32  
Tables S1 and S2  
References (31–34)  
MDAR Reproducibility Checklist  
Submitted 13 March 2023; accepted 19 July 2023  
10.1126/science.adh7726